Development of a hydro kinetic river turbine with simulation and operational measurement results in comparison

A Ruopp[1], A Ruprecht[1], S Riedelbauch[1], G Arnaud[2], I Hamad[2]

[1]Institute of Fluid Mechanics and Hydraulic Machinery; University of Stuttgart, Pfaffenwaldring 10, 70569 Stuttgart, Germany
[2]RER Hydro, 7170 Frédérick-Banting, Saint-Laurent, QC, Canada

ruopp@ihs.uni-stuttgart.de

Abstract. The development of a hydro-kinetic prototype was shown including the compound structure, guide vanes, runner blades and a draft tube section with a steeply sloping, short spoiler. The design process of the hydrodynamic layout was split into three major steps. First the compound and the draft tube section was designed and the best operating point was identified using porous media as replacement for the guide vane and runner section (step one). The best operating point and the volume flux as well as the pressure drop was identified and used for the design of the guide vane section and the runner section. Both were designed and simulated independently (step two). In step three, all parts were merged in stationary simulation runs detecting peak power and operational bandwidth. In addition, the full scale demonstrator was installed in August 2010 and measured in the St. Lawrence River in Quebec supporting the average inflow velocity using ADCP (Acoustic Doppler Current Profiler) and the generator power output over the variable rotational speed. Simulation data and measurements are in good agreement. Thus, the presented approach is a suitable way in designing a hydro kinetic turbine.

1. Introduction

Today's demand for clean and renewable energy is the result of the global warming which is "the human interference with the climate" [1, p. 3], the environmental pollution and the demand for cheap and reliable energy. The renewable energies, especially hydropower, are a growing market facing the challenge to supply the world's increasing electric power demand. Hydropower is one of the most important renewable energy sources, with an amount of 3,402 billion kilowatthours electricity generation in 2010, expected to increase about 83% from 2010 to the year 2040 [2]. The U.S and the Canadian hydropower generation will have some potential to grow, especially in the field of non-dam hydro. First resource assessments indicate a theoretical hydrokinetic power potential of 38,000 MW in Canada and a total potential of 170,000 MW in the U.S.A [3]. The non-dam hydro technology has no need for constructing a dam, which could have drawbacks regarding the ecology in some areas. In addition, this technology seems to be promising for local electrical energy supply in developing countries such that an operation in isolated networks is possible. A second advantage of hydrokinetic machines is their very well predictable power generation.

The politicians in the U.S.A. developed formalities for a first commercialisation of this technology. The Federal Energy Regulatory Commission (FERC) in the U.S.A. issued four preliminary permits for non-dam power generation or so called hydrokinetics. The total capacity of available permits in 2012 was 8,399 MW and increased to 22,340 MW until 2014 [4]. This huge potential is ready for commercialisation.

Many attempts exist for the utilisation of hydrokinetic power. Khan [5] gives an overview about the challenges and possible technical answers. In his following paper he also emphasizes the possibility to duct turbines [6] in order to increase power density at runner stage. River turbines and their development as well as advances and trends are presented in [7] and [8]. Here, turbine settings and generator design are emphasized.

2. Principles of hydrokinetics

The hydrokinetic turbines share the same principal as wind turbines and tidal turbines. The theory for such turbines and the science of making torque from currents can be dated back to the early 1920's where Lanchester first published his theory about propulsion and the screw propeller, where he stated that the maximum power is obtained from a windmill when the residual velocity downwind from the rotor is 1/3 that of free wind [9]. This ideal induction factor $a = 1/3$ leads to the maximum conversion efficiency of $c_p = 16/27$ and is derived by Betz in [10]

$$c_p = \frac{P_{ideal}}{\frac{1}{2}\rho A c_\infty^3}, \tag{1}$$

where P_{ideal} is the extractable power, ρ is the density, A the maximum cross section area and c_∞ is speed of the free fluid flow. Regarding the ideal blockage ratio, Bergey [11] proposed to call it the Lanchester-Betz limit (an elaborately historical presentation of the derivation is given in [12] with yet another suggestion of naming).

The maximum power output depends on the cross section area and the velocity which is cubed. For high power output, deep rivers and high speed currents are needed, where the cross section area can be determined large. The Lanchester-Betz limit indicates that not all available energy can be captured by the turbine since a complete blockage would result in zero volume flux. This fact leads to less power output compared to classical river turbines using a damn equivalent to:

$$P_{theoretical} = \frac{P_{ideal}}{c_p} = \rho g h Q \tag{2}$$

where Q and h denotes the discharge and head respectively. This relationship is illustrated in figure 1 with the theoretical available power versus the ideal power.

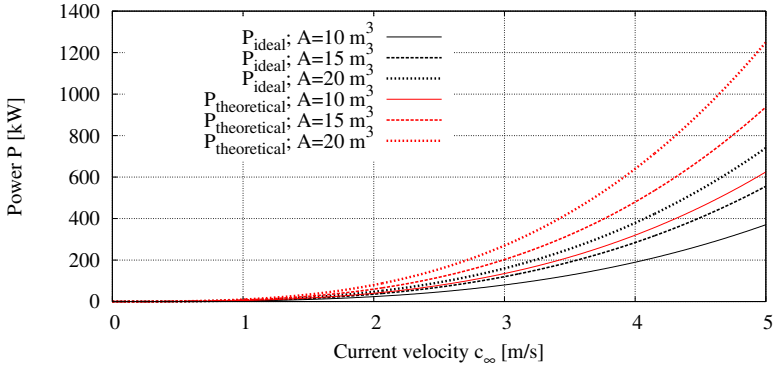

Figure 1. Theoretical and ideal power output for hydrokinetic turbines over undisturbed free flow velocity for three different cross section areas.

The cross section is defined as the projected area of the turbine unit in flow direction impartial from the fact that this area is covered by the turbine itself or the compound structure. This is important for the definition of the power coefficient. The turbine unit itself can be seen as an actuator disk whether it is a horizontal axis free stream turbine unit without a diffusor or a turbine unit using a shroud around the impeller with an adjacent draft tube section, e.g. a turbine with a diffusor.

Several studies exist for using a diffusor to improve turbine power output. Lawn is using a one dimensional approach for simulating several turbines with different diffusors and concludes that there exists an optimum turbine resistance for given diffusor efficiencies [13]. Other studies, such as [14], are using a bypass stream for the power increase. Further studies are using 3D Navier-Stokes solvers replacing the turbine unit with a momentum source model to find the optimum resistance for a diffusor unit [15]. This approach is fast and reliable, since it takes into account the resistance of the turbine unit as well as the losses of the intake and the diffusor region. The losses of the diffusor region can be expressed in terms of the pressure recovery coefficient $c_{p,dt}$, well known from classical hydro power units for draft tubes, e.g. elbow draft tubes (Δp_{static} is the static pressure difference from outlet to inlet, $c_{dt,inlet}$ denotes the mean velocity at draft tube section inlet):

$$c_{p,dt} = \frac{\Delta p_{static}}{\frac{\rho}{2} c_{dt,inlet}^2} \tag{3}$$

Among this work there exist experimental data, which prove the concept of diffusors e.g. Reinecke [16] and Birjandi [17]. Reinecke uses the turbine cross section area for calculating the conversion efficiency resulting in transgression of the Lanchester-Betz limit. Birjandi shows the influence of blockage effect and free surface influence on power characteristics, which indicates, that it is important to minimise those influences in the hydraulic design stage.

Experimental and simulation data for a turbine with optimised diffusor is given in [18]. Here, the influence of blockage effect is visible in the experiment resulting in higher conversion efficiency than the Lanchester-Betz limit. However the Lanchester-Betz limit cannot be exceeded when taking into account the correct definition of the cross section area plus eliminating secondary blockage effects from small laboratory flumes or small computational domains.

However, the use of a diffusor can be beneficial. The application of hydrokinetics in rivers is mostly restricted by the available vertical space. In such a case, non-axis symmetric draft tubes can increase the cross section area compared to a non-shrouded axis-symmetric horizontal axis turbine layout, shown in figure 2.

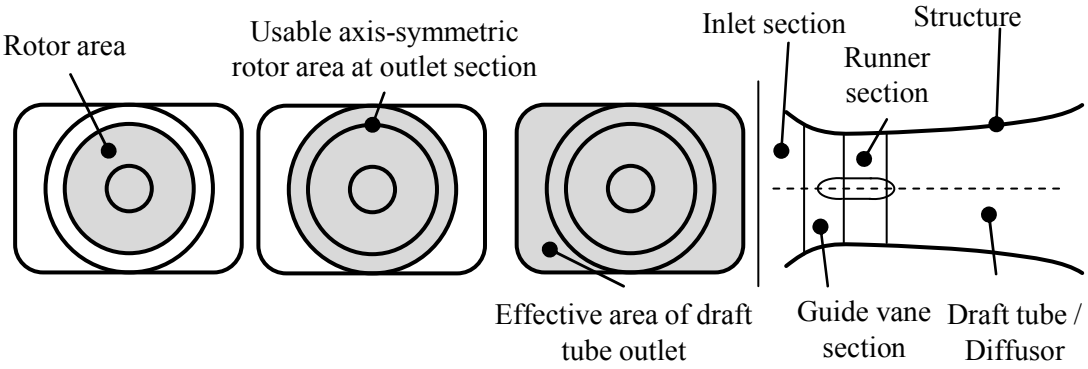

Figure 2. Rotor area, axis-symmetric rotor area and effective cross section area for non-axis symmetric case as well as base layout for the prototype (from left to right).

In addition, the river depth is not the only limitation for the turbine unit dimension; it is also affected by external influences like waves, boats, ice as well as possible boundary layer effects caused by the rough bottom surface. The horizontal extension of the draft tube is mostly not limited and can be utilized by a non-axis symmetric layout. Further attributes are the rise of power density in the rotor area which can be used for smaller rotor diameter, higher runner speeds resulting in smaller generators and ensuring a more stable operation of the runner caused by possible disturbance in upstream flow.

3. The TRÉC prototype turbine

The base layout of the TRÉC (Turbine de Recupération de l'Energie Cinétique) prototype turbine consists of an inlet region, a guide vane section, a runner section with a following non-axis symmetric draft tube (figure 2, on the right). Table 1 summarizes the design data.

Table 1. Design data of TRÉC prototype turbine

Maximum power	350	kW
Water velocity	1.5-4.5	m/s
Generator	Variable Speed with frequency converter	
Guide vanes	5 fixed blades	
Runner	4 fixed blades	
Diameter of turbine	2.8	m

Major goal is a robust and reliable turbine layout reducing the maintenance. The turbine uses a horizontal axis, shrouded turbine with fixed guide vanes and fixed runner blades. The generator uses an outer ring. Ensuring a higher stiffness between rotor blades and generator ring, four runner blades are utilized instead of three.

3.1. Demonstrator Installation and Operation

The turbine was manufactured in 2010 and installed in the Saint Lawrence River in Montreal (installation date was August 18th, 2010). A jack-up barge was utilized upstream; a swimming barge with crane and turbine was fixed to the jack-up barge. A tugboat was additionally used to stabilise the swimming barge for security reasons, figure 3. Instead of using a fixed fundament, the turbine foundation consist of 4 adjustable piles, which can be adjusted in length enabling a horizontally and stable positioning of the turbine.

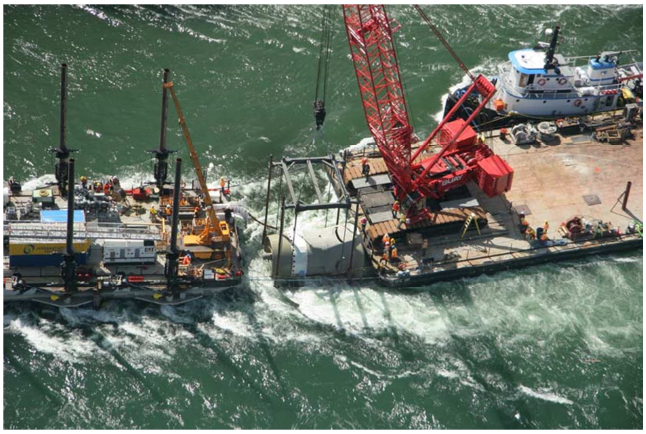

Figure 3. Installation of full scale demonstrator / prototype in the Saint Lawrence River in Montreal with jack-up barge (left), prototype (in the middle), swimming barge (right).

3.2. Measurement setup

The measurements are taken at turbine position before installation. The free stream velocity range is between 2.6 and 3.25 m/s in average, figure 4. The arithmetic average value is taken as boundary condition for the simulation setup. The high scatter of each single velocity profile over height indicates a high turbulence in the flow regime.

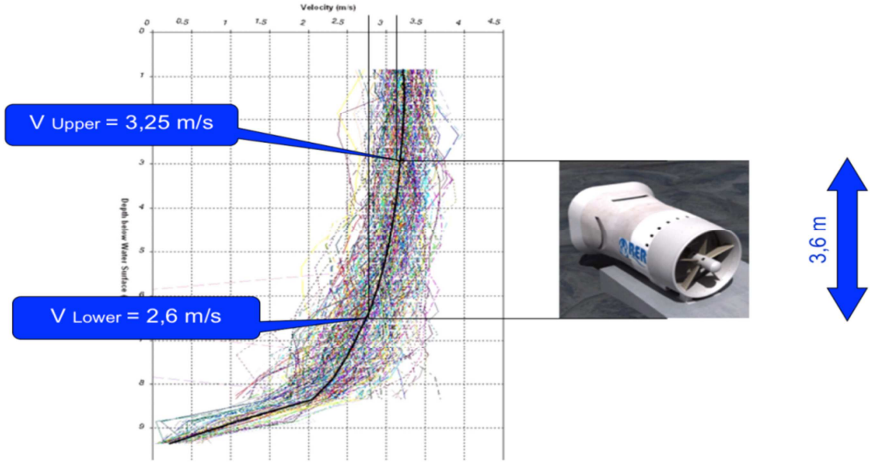

Figure 4. Velocity field at turbine position measured with ADCP over water height. Inflow height is 3.6 m (right).

3.3. Hydraulic development

The complete hydraulic design phase is split into three major parts. In the early design phase (phase I), the compound structure and the hub was modelled without runner blades and guide vanes to determine the size of the computational domain, to ensure grid independence and to detect the best operating point including volume flux and pressure difference at turbine stage. In this case, the turbine unit (guide vanes and runner blades) are replaced with an isentropic loss in the numerical model, e.g. a porous domain incorporating an ideal loss. This ideal loss is causing a pressure drop in the turbine section. While increasing this loss, volume flux is decreasing, pressure drop is increasing. The power

can be determined with the pressure loss $\Delta p_{s,pd}$ between porous inlet and outlet (runner area) and the volumetric flux Q_{pd}.

$$P_{ideal} = \Delta p_{s,pd} Q_{pd} \tag{4}$$

The loss of the porous media can be determined with a first assumption, that the ideal induction factor is reducing the velocity speed at outlet of draft tube section to

$$c_{dt} \approx \frac{2}{3} c_{\infty}. \tag{5}$$

With the continuity equation, the velocity at turbine section c_t is calculated to

$$c_t = \frac{A_{dt}}{A_t} c_{dt}. \tag{6}$$

The isentropic loss is causing a resistant force F_{pd} with

$$F_{pd} = \frac{\rho}{2} A_t \underbrace{c_{pd}}_{l_c \Delta s} c_t^2. \tag{6}$$

where A_t is the turbine section area, c_{pd} the drag coefficient, l_c the loss coefficient and Δs the length of the porous domain. This first assumption of loss coefficient can be used as an initial value for the numerical setup. With this approach the ideal operation can be identified in a few steps. All steady state CFD runs are performed using the k-Omega SST turbulence model.

3.3.1. Domain size and grid independency

The correct domain size is varied to exclude the blockage effect of boundaries and to eliminate the influence of inlet and outlet boundaries onto the power characteristics of the turbine unit. The goal is a constant peak power while increasing the boundary distance to the turbine unit. The domain size is varied with a constant factor f_{domain} by multiplication of the distance from the boundaries to the turbine unit. In total four different domain sizes are simulated while increasing the domain with every extension. The variation of the domain size leads to a stagnation of peak power performance (figure 6). The following simulation runs are using the largest setup to ensure that the influence of the domain size is insignificant on the power characteristics. The final domain has the following dimensions (in total): Total length from inlet to outlet is 365 m, width is 280 m and height from top to machine axis measures 60 m (figure 5).

The influence of the mesh size is carefully examined since a rough mesh setup is leading to higher power output in these cases. In detail, mesh size, mesh topology and wall mesh resolution for the boundary layer is varied. In total, 5 different mesh setups are simulated for three different turbine unit geometries and 5 different operation points (loss coefficients).

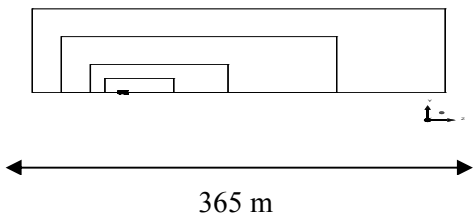

Figure 5. Domain sizes in top view (compound length 8m).

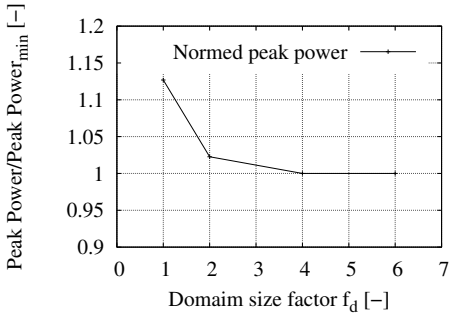

Figure 6. Influence of domain size on normed peak power over scaling factor of domain extension.

For all simulation runs, a block-structured hexahedral mesh setup is used. The final mesh setup consists of 7.190.000 nodes with y+-values between 5 and 11 for the compound walls.

The grid independency is shown in figure 7 for five different mesh setups. The mesh resolution around the draft tube as well as the wake region behind the spoiler is detected as a main driver for the power characteristic.

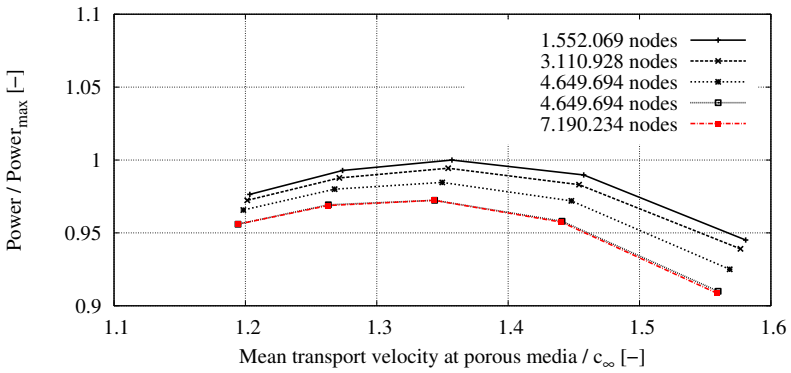

Figure 7. Normed peak power versus velocity ratio (transport velocity at porous domain / free flow velocity) for different mesh setups, final mesh setup highlighted with red.

3.3.2. Design of compound and draft tube section

The compound design and the draft tube section are performed with the porous domain setup, i.e. without the guide vanes and the runner blades. To speed up the design process, a free surface model is neglected and, instead, a free slip surface is used. Different loss coefficients are simulated to detect the best operation point. In detail, several draft tube designs are investigated with respect to the inner slope (opening angle), the angle of the spoiler region as well as the horizontal extension of the draft tube outlet. The draft tube has no separation with an inner slope below 4 degrees and using a rampant spoiler with a slope of at least 20°. In the later design phase with guide vanes and runner blades, slots are used to stabilize the flow in the draft tube section ensuring the prevention of separation. The presented compound structure with the draft tube reaches almost the target power, figure 8.

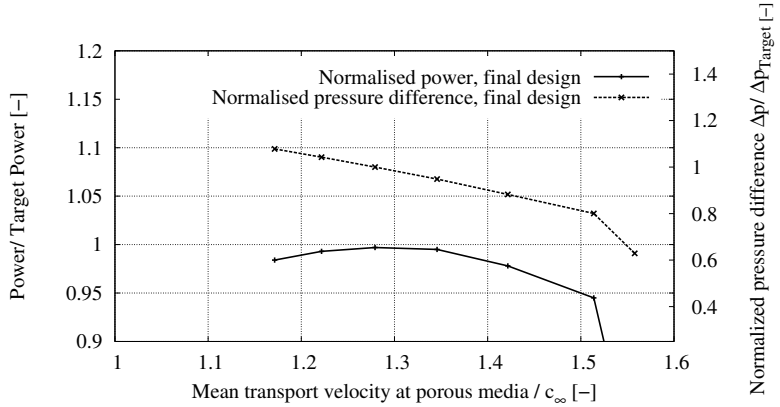

Figure 8. Normed power (left ordinate) versus velocity ratio (transport velocity at porous domain / free flow velocity) and normalised pressure difference versus porous domain (right ordinate).

The sudden pressure drop and resulting power decrease for operating point with high velocity ratios (figure 8) is caused by a separation in the draft tube, which is a beneficial side effect when turbine operates in over speed and power needs to be limited. Around the best operating point the draft tube pressure recovery and peak power do not collapses over a fairly wide operation range, figure 9.

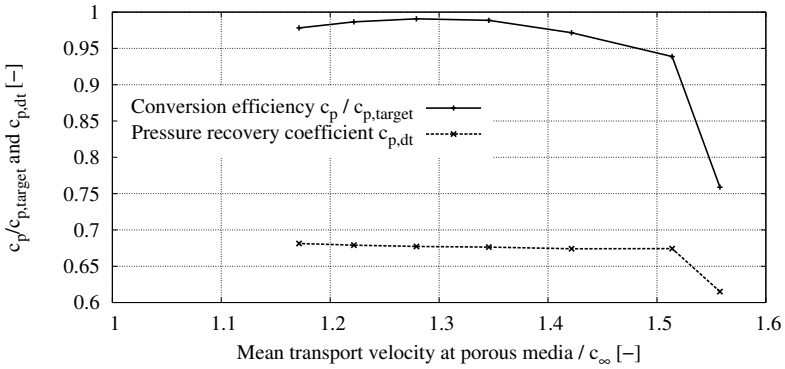

Figure 9. Pressure recovery coefficient of draft and conversion efficiency ratio versus velocity ratio (transport velocity at porous domain / free flow velocity).

3.3.3. Design of guide vanes and runner blades

The volumetric flux and pressure difference from design phase one are used to develop the guide and runner blades. Previous studies showed that a single rotor without guide vanes is influencing the flow characteristics in the draft tube section negatively. This can be ascribed to the circumferential velocity field downstream of the runner, which causes instabilities in the non-axis symmetric draft tube. Therefore, and for stiffness reason, a setup with guide vanes are chosen with five blades.

The guide vanes and the runner blades are designed to obtain a constant iso-energetic work distribution with

$$r \cdot c_u = const. \tag{7}$$

For both, guide vane and runner blades a single channel (channel to channel) with a periodic setup is used to simulate and control target circumferential velocity distribution. In detail, a symmetric NACA series is used as base and a polynomial camber line is superimposed in order to meet relative inflow and outflow angles. The absolute thickness distribution is fixed ensuring stability of the blades.

The mean velocity field at the exit of guide vane section is used as inlet boundary condition for the runner simulation setup. Here, the circumferential velocity field is converted to torque; target is the absence of a circumferential velocity component at the exit of the runner. The sum of pressure difference of both, guide vanes and runner, must meet the peak operating point of design stage one to ensure the best velocity ratio of 1.3. Otherwise the blockage of turbine unit would not be optimal.

3.3.4. Comparison of simulation data and measurements

The complete turbine is simulated using stationary simulation runs without the mounting part and support struts after the runner section. The domain setup and its extension are identical as described before. The normalized power curves are given in figure 10. The steady state simulation runs capture the power characteristics of the measurements. In detail, the hydraulic power is corrected with a total efficiency known from secondary losses like generator loss, cable losses, bearings and direct driven oil pump. Nevertheless, the sudden brake of power above design point is not captured in the simulation

run due to the fact that the additional swirl behind the rotor is not causing a separation in the draft tube section because of the absence of the supporting struts.

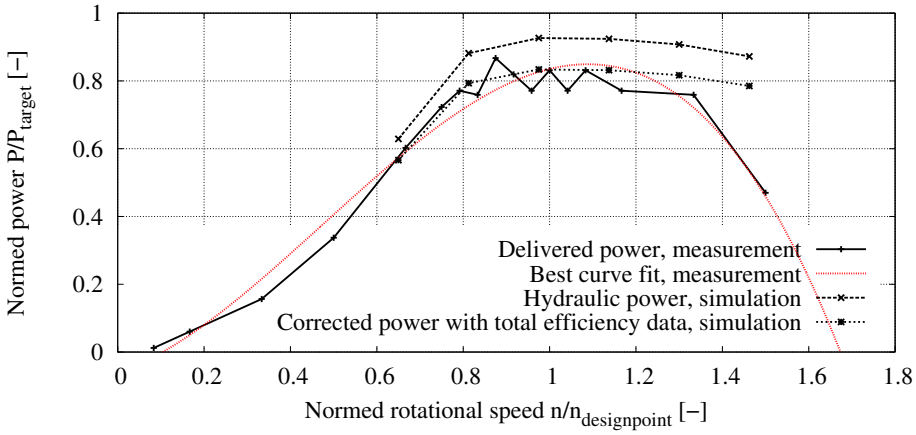

Figure 10. Normed power over normed rotational speed for hydraulic power, corrected hydraulic power and measured electrical power with curve fit.

4. Conclusions

The design of a hydrokinetic turbine is presented using three sequential steps. The use of an isentropic loss (e.g. porous domain) is a suitable way in identifying major characteristics of shrouded turbines with diffusors or draft tubes. Pressure drop, peak power and volumetric fluxes are captured accurately and provide an ideal basis for the design of runner and guide vanes. The use of a non-axis symmetric draft tube induced a setup with guide vanes. Otherwise, the swirl component would cause separation at supporting struts and in the draft tube section in this case. The installation of the prototype and the operation is successfully performed and the full scale demonstrator is running without any downtime since installation in August, 2010. The predicted power output from CFD is in good agreement to the measured electrical power.

References

[1] IPCC 2014 Climate Change 2014: *Impacts, Adaption and Vulnerability – Summary for policy makers*, Technical Support Unit, Carnegie Instituion for Science, 2014
[2] International Energy Agency 2013, *World Energy Outlook, International Energy Agency*, Web. July 2013
[3] Briand, M-H, Ng, K 2010, *Kinetic Energy Recovery Turbine Technology: Resource Assessment and Site Development Strategy, World Energy Conference*, Montreal, Canada, 13-17 September 2010
[4] FERC (25.4.2014) http://www.ferc.gov/industries/hydropower/gen-info/licensing/hydrokinetics.asp
[5] Khan M, Iqbal M, Quaicoe J 2008 *River current energy conversion systems: Progress, prospects and challenges*, Renewable and Sustainable Energy Reviews, 2008, 12, 2177-2193
[6] Khan M J, Bhuyan G, Iqbal M T, Quaicoe J.E. 2009 *Hydrokinetic energy conversion systems and assessment of horizontal and vertical axis turbines for river and tidal applications: A technology status review*, Applied Energy, 2009, 86, 1823-1835
[7] Güney M, Kaygusuz K 2010 *Hydrokinetic energy conversion systems: A technology status review*, Renewable and Sustainable Energy Reviews, 2010, 14, 2996-3004
[8] Lago L, Ponta F, Chen L 2010 *Advances and trends in hydrokinetic turbine systems*, Energy for Sustainable Development, 2010, 14, 287-296

[9] Lanchester F W 1915 *A contribution to the theory of propulsion and the screw propeller*, Transaction of the Royal Institution of Naval Architects, 1915, 57
[10] Betz A 1920 *Das Maximum der theoretisch möglichen Ausnutzung des Windes durch Windrotoren (The maximum of the theoretical possible exploitation of the wind by wind motors)* Zeitschrift für das gesamte Turbinenwesen, 1920, 26, 307-309
[11] Bergey K 1979 *The Lanchester-Betz limit (energy conversion efficiency factor for windmills)*, Journal of Energy, American Institute of Aeronautics and Astronautics, 1979, 3, 382-384
[12] Okulov V L, van Kuik G A 2012 *The Betz-Joukowsky limit: on the contribution to rotor aerodynamics by the British, German and Russian scientific schools*, Wind Energy, John Wiley & Sons, Lth, 2012, 15, 335-344
[13] Lawn C J 2003 *Optimization of the power output from ducted turbines*, Proceedings of the Institution of Mechanical Engineers, Part A: Journal of Power and Energy, 2003, 217, 107-117
[14] Grassmann H, Bet F, Ceschia M, Ganis M 2004 *On the physics of partially static turbines*, Renewable Energy, 2004, 29, 491-499
[15] Gaden D L, Bibeau E. L. 2010 *A numerical investigation into the effect of diffusers on the performance of hydro kinetic turbines using a validated momentum source turbine model*, Renewable Energy, 2010, 35, 1152-1158
[16] Reinecke J, Backström T, Venter G 2011 *Effect of a Diffuser on the Performance of an Ocean Current Turbine*, 9th European Wave and Tidal Energy Conference (EWTEC), 2011
[17] Birjandi A H, Bibeau E L, Chatoorgoon V, Kumar A 2013 *Power measurement of hydrokinetic turbines with free-surface and blockage effect*, Ocean Engineering, 2013, 69, 9-17
[18] Luquet R, Believre D, Freéchou D, Perdon P, Guinard P, Goujon G 2011 *Design and model testing of an optimised ducted marine current turbine*, 9th European Wave and Tidal Energy Conference (EWTEC), 2011